



Supplement of

Dynamic and thermodynamic processes related to sea-ice surface melt advance in the Laptev Sea and East Siberian Sea

Hongjie Liang and Wen Zhou

Correspondence to: Wen Zhou (wen_zhou@fudan.edu.cn)

The copyright of individual parts of the supplement might differ from the article licence.

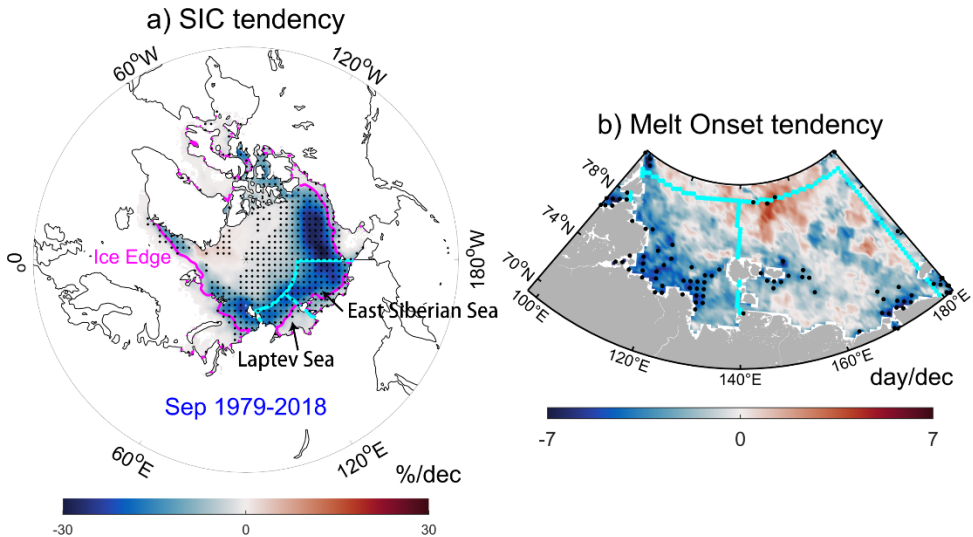


Fig. S1. Arctic sea ice concentration tendency in September, and melt onset tendency in the Laptev Sea and East Siberian Sea (1979-2018). The magenta line in subplot (a) denotes the average ice edge in September. The cyan lines in subplots (a) and (b) are the same as the boundaries of the Laptev Sea and East Siberian Sea. Stippling denotes 95% confidence for the tendency.

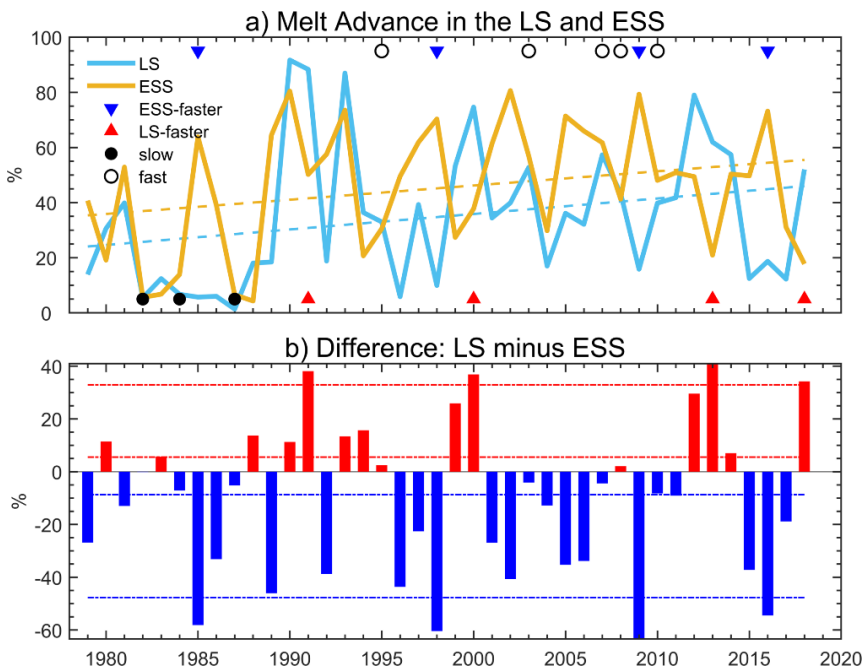


Fig. S2. Melt Advance (MA) and its difference between the Laptev Sea (LS) and East Siberian Sea (ESS), 1979-2018. Subplot (a) is the same as Fig. 1c. In subplot (b), positive difference indicates faster MA in the LS than in the ESS. Dashed lines represent one standard deviation for the red and blue bars, respectively.

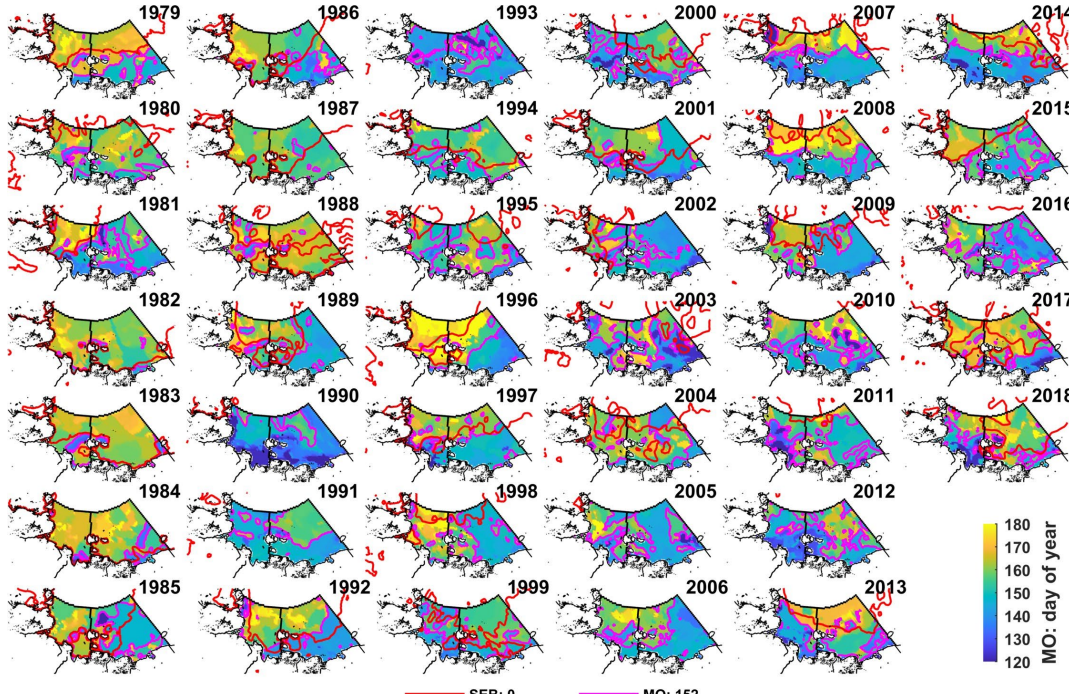


Fig. S3. Sea ice surface Melt Advance and surface energy balance in the Laptev Sea and East Siberian Sea, 1979–2018. For surface energy balance (SEB), only the zero contours are marked by red lines. Melt Advance is represented by the magenta contours of 152 (day of year), with colored shading denoting sea ice Melt Onset (MO).

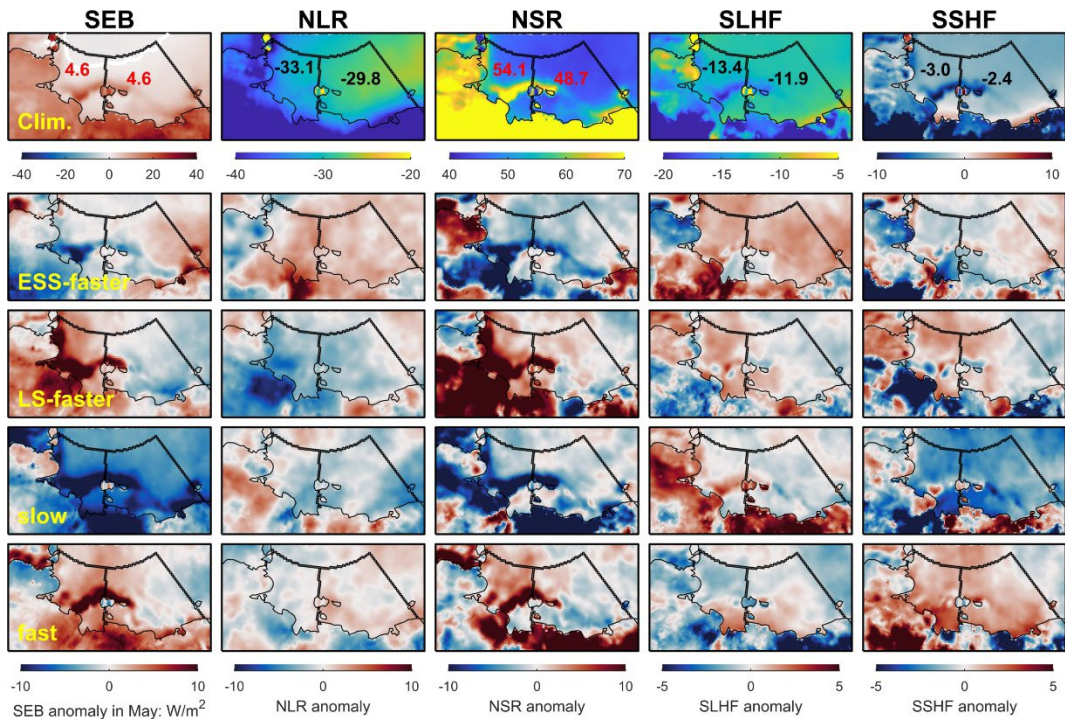


Fig. S4. Climatological distribution of surface energy balance components in May (first row) and composite anomalies for the four scenarios (lower four rows). The relevant variables include SEB, NLR, NSR, SLHF, and SSHF in May, respectively. Numbers within the LS and ESS are the region-mean values for each sea.

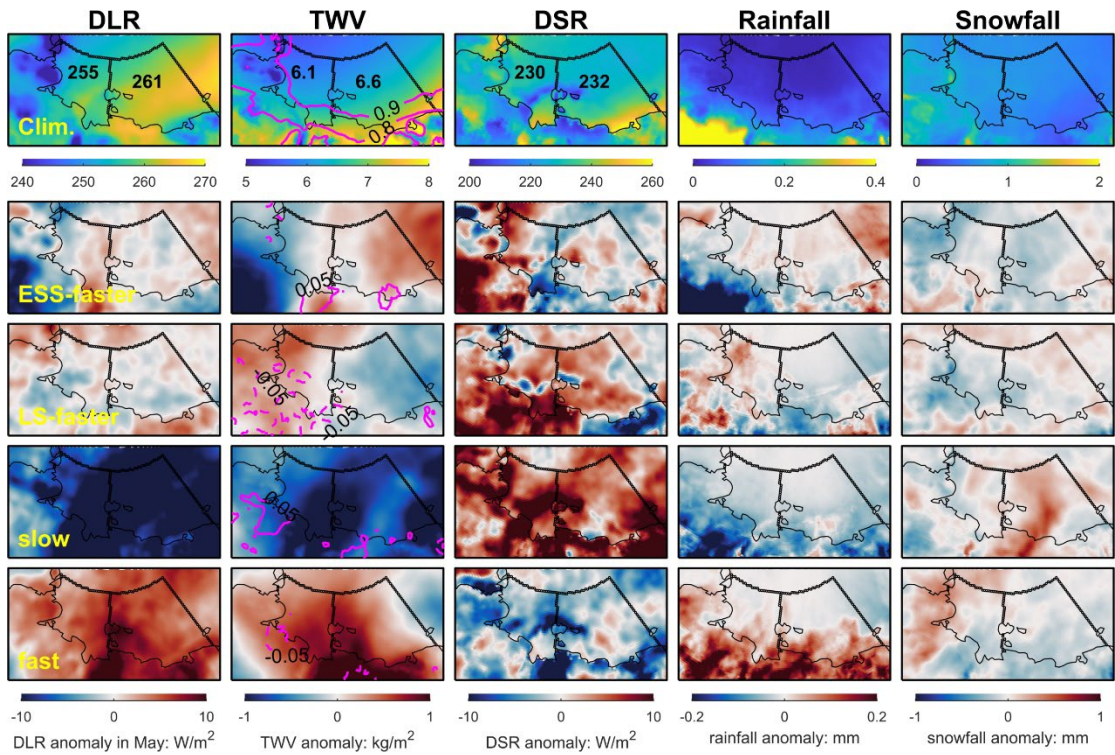


Fig. S5. The same as Figure 4 except for downward longwave radiation (DLR), total-column water vapor (TWV), downward shortwave radiation (DSR), rainfall and snowfall. Magenta contour lines superimposed upon TWV fields denote the corresponding total cloud cover in May.

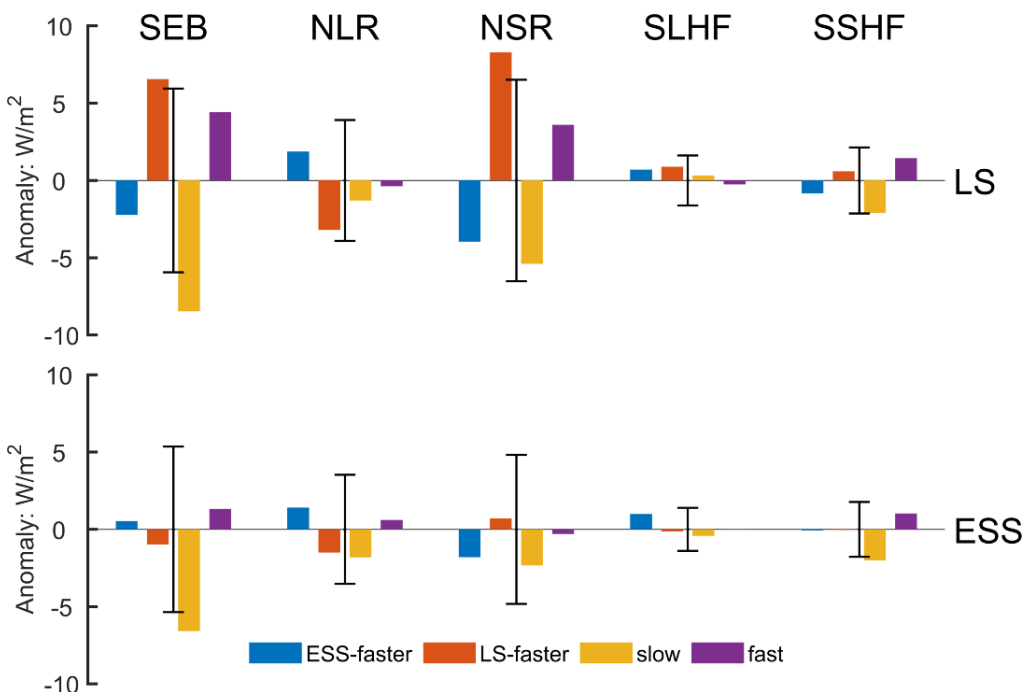


Fig. S6. Region-mean composite anomalies of the surface energy fluxes for each of the four scenarios in the LS and ESS, respectively. The error bars denote the standard deviation for 1979-2018.

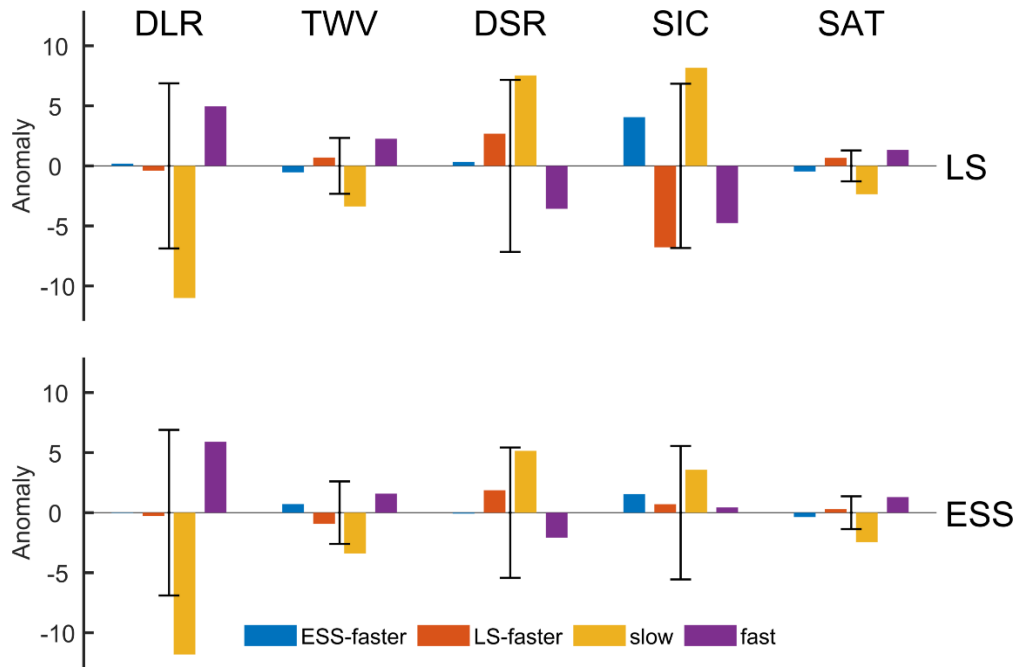


Fig. S7. The same as Figure 5, but for DLR, TWV, DSR, SIC, and SAT, with units of W/m^2 , kg/m^2 , W/m^2 , %, and K, respectively. To facilitate viewing, TWV and SIC are scaled by a factor of 4 and 2, respectively. SIC represents areal percentage of sea ice cover relative to the whole sea.

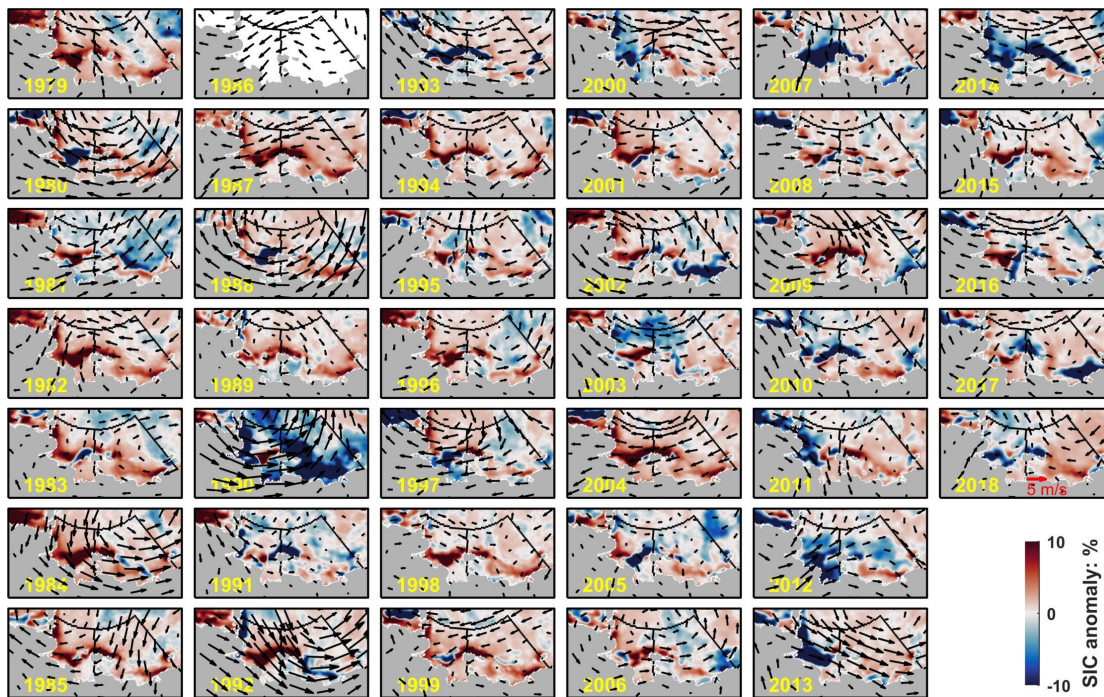


Fig. S8. Anomalies of sea ice concentration and wind fields at 850 hPa in May for 1979–2018. Sea ice concentration in 1986 is missing in the OSI SAF dataset.

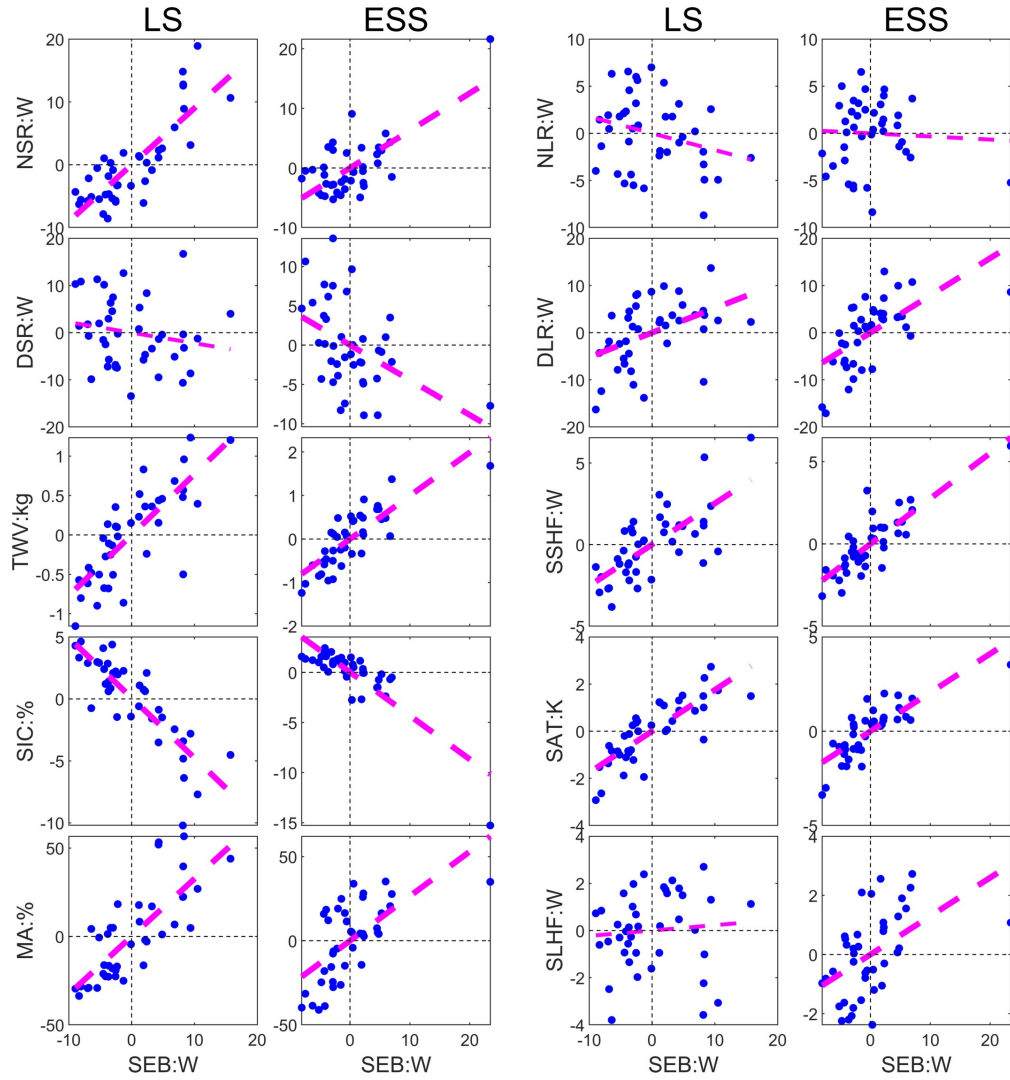


Fig. S9. Scatter plots of region-mean anomalies of SEB and related factors in May in the LS and ESS, including NSR, DSR, TWV, SIC, MA, NLR, DLR, SSHF, SAT, and SLHF, respectively. Dashed magenta lines denote linear fits which are above the 95% confidence level when the lines are thick.